



Published in final edited form as:

Adv Drug Deliv Rev. 2019 January 01; 138: 293–301. doi:10.1016/j.addr.2018.12.007.

Superparamagnetic Iron Oxides as MPI Tracers: A Primer and Review of Early Applications

J.W.M. Bulte, Ph.D.*

Russell H. Morgan Department of Radiology and Radiological Science, Division of MR Research, Cellular Imaging Section and Vascular Biology Program, Institute for Cell Engineering, Department of Chemical & Biomolecular Engineering, Department of Biomedical Engineering, and Department of Oncology, The Johns Hopkins University School of Medicine, Baltimore, MD 21205, USA

Abstract

Magnetic particle imaging (MPI) has recently emerged as a non-invasive, whole body imaging technique that detects superparamagnetic iron oxide (SPIO) nanoparticles similar as those used in magnetic resonance imaging (MRI). Based on tracer “hot spot” detection instead of providing contrast on MRI scans, MPI has already proven to be truly quantitative. Without the presence of endogenous background signal, MPI can also be used in certain tissues where the endogenous MRI signal is too low to provide contrast. After an introduction to the history and simplified principles of MPI, this review focuses on early MPI applications including MPI cell tracking, multiplexed MPI, perfusion and tumor MPI, lung MPI, functional MPI, and MPI-guided hyperthermia. While it is too early to tell if MPI will become a mainstay imaging technique with the (theoretical) sensitivity that it promises, and if it can successfully compete with SPIO-based ^1H MRI and perfluorocarbon-based ^{19}F MRI, it provides unprecedented opportunities for exploring new nanoparticle-based imaging applications.

Keywords

Magnetic particle imaging; magnetic resonance imaging; superparamagnetic iron oxide; nanoparticles; tracer; cell tracking; molecular imaging

1. Introduction

1.1. The dawn of MPI

MPI is a novel non-invasive imaging modality, although the technology itself is not new. MPI was invented in 2001 by Gleich et al. at Philips Research Hamburg GmbH [1]. Four

*Corresponding author at: Russell H. Morgan Department of Radiology and Radiological Science, Division of MR Research; Cellular Imaging Section and Vascular Biology Program, Institute for Cell Engineering, The Johns Hopkins University School of Medicine, 217 Traylor Bldg, 720 Rutland Ave, Baltimore, MD 21205.

Publisher's Disclaimer: This is a PDF file of an unedited manuscript that has been accepted for publication. As a service to our customers we are providing this early version of the manuscript. The manuscript will undergo copyediting, typesetting, and review of the resulting proof before it is published in its final citable form. Please note that during the production process errors may be discovered which could affect the content, and all legal disclaimers that apply to the journal pertain.

years later, in 2005, the scientific world first heard about MPI [2]. Since Philips is not a vendor of preclinical systems and did not want to enter this market, the company then licensed its MPI business to Bruker Biospin AG, who released the first commercial pre-clinical scanner in 2013. Around 2007, Drs. Conolly and Goodwill, then at Stanford University and later at UC Berkeley, developed a series of alternative MPI scanner prototypes based on the same basic MPI principles except for (2D) data acquisition and zero field-based image reconstruction [3]. Around 2014, Magnetic Insight Inc. was founded as the second company to bring an MPI scanner to the market, which was introduced in New York at the World Molecular Imaging Conference in 2016 (Figure 1).

1.2. Simplified principles of MPI

A common mistake in the current literature is to call superparamagnetic iron oxide (SPIO) nanoparticles MPI “contrast agents”. Contrast is defined as the difference between two signal intensities. Since there is no background MPI signal present in tissue before SPIO administration, there is no contrast. This is unlike MRI, where we always have proton signal before SPIO injection; hence the term contrast agent does apply. Instead, SPIOs are “MPI tracer agents”, similar to radioactive tracer agents or isotopes that are detected directly in nuclear medicine, without any background signal from tissue. In analogy, there are no “radioactive contrast agents”, only radiopaque contrast agents as known from computed tomography.

The MPI technology is based on the principle that SPIO nanoparticles can be magnetized by an external magnetic field and exhibit a nonlinear response in a near-zero magnetic field. When the external field changes around the value 0, the magnetization will follow until it reaches a positive or negative saturation value for larger positive or negative magnetic fields. In the basic MPI scanner setup, a magnetic gradient field is created in such a manner that there is only 1 point in the 3D imaging volume at any given time at which the magnetic field is zero. Only at this point, the so-called “field-free point” (FFP), will it be possible to observe oscillating changes in magnetization if an additional, oscillating external magnetic field is applied (typically in the kHz range). These changes are then detected via magnetic induction in a sensing radiofrequency coil, much like in MRI, and following spatial reconstruction MP images can be created. An alternative method is to apply a “field-free line” (FFL) [3] instead of multiple FFPs to obtain increased sensitivity, but at the cost of temporal resolution.

2. SPIOs as MRI contrast agents

2.1 Established MRI applications

Although magnetic nanoparticles were reported to have the ability to shorten MR T2 relaxation times in the late 70s [4], SPIO contrast agents did not make their introduction as MRI contrast agents until the 1980s [5–7]. It was realized that these nanosized magnetic entities change the microenvironment of the strong external magnetic fields, leading to a loss of phase coherence of resonating protons with as result a loss of MRI signal [8]. Since then, their primary clinical use has been as negative contrast agents for liver and lymph node imaging [9], where normal tissue contains an abundance of phagocytic cell types that take up

injected SPIO particles and turn black on MRI, whereas pathological tissue shows a reduced uptake and lack of contrast due the reduced number of Kupffer cells or macrophages.

Many of the established applications that MRI has seen for SPIO contrast agents will surely be revisited with MPI. As further detailed below, one such application is tracking of cell transfer and transplantation [10], where cells are pre-loaded with SPIO *in vitro* before administration. Another example is imaging of inflammation, following intravenous injection of nanoparticles that accumulate in macrophages at the site of inflammation [11].

2.2. MRI limitations

Although SPIO MR contrast agents are the most effective MRI contrast agents known today, with field-dependent T2 relaxivities well exceeding $>100 \text{ mM}^{-1}\text{s}^{-1}$ [12], they have several drawbacks. Most prominent among these is their nanoparticle nature, which causes their rapid elimination from the bloodstream through non-specific uptake by phagocytic host cells. This has prevented their overall use as more specific, targeted agents such as those widely used in nuclear medicine. Secondly, the contrast agents create “black holes”, obscuring the underlying anatomical tissue structures. In addition, other endogenous sources of contrast may be confused with the exogenous SPIO particles, such as the existence of hemorrhage (iron deposits), air-tissue interfaces (skin surface, lung tissue, bowel content) and/or motion and static magnetic field imperfections. Third, since SPIO is not directly detected but indirectly through its relaxation effects on protons, it is not possible to reliably quantify the local tissue concentration of SPIO particles. As further described below, some of these limitations are not encountered in MPI.

3. SPIOs as MPI tracers

3.1. Early MPI applications

3.1.1. MPI cell tracking—One of the earliest SPIO MRI applications has been in cell tracking [13–15], and the same can be said for MPI [16, 17]. In order to test the hypothesis that MPI is truly quantitative, since it detects SPIO particles directly, smaller cell bodies (neural stem cells – NSCs, diameter approximately $10 \mu\text{m}$) and larger cells (mesenchymal stem cells – MSCs, diameter approximately $25 \mu\text{m}$) were labeled with three different SPIO preparations, i.e, the MRI contrast agents Resovist and Feridex, as well as MPI-optimized particles [18]. Magnetic particle spectroscopy (MPS) measurements demonstrated a linear correlation between MPI signal and iron content, for both homogeneous solutions of free particles in solution and for internalized and aggregated particles in labeled cells over a wide range of concentrations (Figure 2). The fact that SPIO produces the same MPI signal per unit of iron, regardless of its intra- or extracellular conformation, is important as for *in vivo* MPI applications the biological conformational state of SPIO particles in tissue is often not known *a priori*. For instance, particles can be present as free (unbound) entities within the interstitial fluid, as single bound particles to cell surface receptors, or as large combined particle clusters inside cells in endosomes. With MRI, these different conformational states lead to different relaxation regimes, as larger clusters are less effective in spin-spin (T1) relaxation and tend to lead to dominant T2* and magnetic susceptibility effects.

To further test SPIO-labeled cell quantification in tissue, four different quantities of SPIO-labeled MSCs were stereotactically transplanted in the striatum of mouse brain (100,000, 50,000, 25,000, and 10,000 cells). Using the initial Philips pre-clinical MPI prototype scanner at Philips Research, Hamburg, Germany, cells could be readily detected by MPI at a detection threshold of about 5×10^4 cells, with MPI/MRI overlays showing a good agreement between the hypointense MRI areas and MPI hot spots (Figure 3) [19]. The calculated tissue MPI signal ratio for 100,000 vs. 50,000 implanted cells was 2.08, in close agreement with the 2-fold difference in cell number, confirming proper tracer quantification with MPI.

Around the same time, initial MPI cell tracking studies were performed by the Berkeley group. Using MSCs, it was demonstrated that SPIO-labeled NSCs could be detected by MPI in rat brain, and that the particles persisted for several months [20]. Systemically injected SPIO-labeled MSCs initially became entrapped within the lung vasculature, and then redistributed within one day to the liver and spleen (Figure 4)[21], which is a typical distribution pattern previously observed with single photon emission computed tomography (SPECT) of intravenously injected ^{111}In -oxine-labeled MSCs in both small [22] and large [23] animal models. The resulting “hot spot” MP and SPECT images are very similar in appearance and allow analysis of distribution in the lung, which is not possible with MRI using SPIO-labeled cells. Others have applied MPI cell tracking for visualization of SPIO-labeled islets engrafted in the liver and kidney capsule, where further cellular MPI quantification was demonstrated [24]. While Resovist and Feridex have similar T2 relaxivities and are approximately equally effective as MRI contrast agents, they have different performances in MPI as shown for both free particles and when internalized in cells [19]. With the optimal performance dictated by the magnitude of the superparamagnetic moment and uniform crystal size, attempts are underway to develop fine-tuned SPIO formulations with optimal MPI properties for cell tracking. One example is to synthesize Janus iron oxide nanoparticles that are three times more effective compared to Resovist and 7 times more compared to Feraheme [25]. It has been reported that MPI can have extreme high sensitivity, in the order of <1 pg within the entire FOV [26]. Since cells labeled with SPIO for MRI cell tracking purposes have an average iron content of 5–10 pg Fe/cell, one can in theory track a single cell with MPI. While the early field of MPI cell tracking has not shown this feasibility yet, an *in vivo* sensitivity of 250 cells within the FOV of an entire mouse has been reported using these MPI-optimized Janus iron oxide nanoparticles [25]. As for MRI, single cell tracking has only been possible when using labeling with non-clinical formulations of very large magnetic microspheres [27, 28]. Since these studies have used very small FOV's for brain or liver (not whole mouse FOV), with each cell containing >100 -fold iron content, these MRI studies do not allow a proper comparison for its sensitivity of MPI. Multi-modal MPI cell tracking agents are now also being developed, although at the cost of a lower sensitivity in the order of 1 million cells [29].

3.1.2. Multiplexed MPI—Using different SPIO particle types with different magnetic responses (MPI frequency harmonics), it is possible to selectively sample the signal from each particle subtype and assign artificial colors so that one can perform “multi-color imaging [30–33]. Aside from temperature mapping [34], this creates unprecedented opportunities to study multiple cell subtypes or targeted molecules simultaneously, *in vivo*,

within their biological context (i.e., to study the interaction of tumor cells with host stromal cells). This approach can be compared to multi-color paraCEST (chemical exchange saturation transfer) MRI using two different paramagnetic agents [35] or diaCEST MRI using two different diaCEST agents [36], but there are no potentially toxic metals involved (as in the case of paraCEST MRI) and there is no background contrast (unlike the case of diaCEST MRI) that may complicate image interpretation.

3.1.3. Perfusion and tumor MPI—(U)SPIO particles have been used with MRI early on for perfusion imaging [37] and the detection of leaky endothelium in the case of blood-brain barrier disruption [13]. MPI cerebral perfusion scans have been performed in stroke [38] and traumatic brain injury [39], and has shown its utility for unambiguous detection of neuropathological changes (Figure 5). With the high temporal resolution of 40 frames per second for the FFP method, flowing blood can be observed in real-time in the heart [40] and the brain [38], and it is possible to obtain blood flow velocity measurements [41]. Notably, MPI was able to differentiate the anterior and posterior cerebral circulation via the basil artery, which was not occluded in the MCAO model where it showed an unimpaired perfusion (Figure 5A). Given their nanoparticle size, SPIO particles will not leak out of blood vessels unless they are compromised. This has been exploited for detection of internal bleeding in a rat traumatic brain injury (TBI) model, where large hemorrhagic areas could be identified (Figure 5B). While SPIO nanoparticles generally clear quickly and for-real time perfusion imaging bolus injections need to be performed followed by rapid MPI acquisition, the particles can be encapsulated inside red blood cells to prolong their clearance and to turn them into long-term blood pool imaging agents [42–44], for a period of 30 days which is the natural half-life of erythrocytes.

For several reasons, fast growing tumors benefit from leaky vessels with larger pore sizes, enabling a quick exchange of nutrients. This biological feature has previously been exploited to non-selectively target tumors with SPIO nanoparticles [45] and other nanosized contrast agents [46, 47] by means of the so-called enhanced permeability and retention (EPR) effect, leading to enhanced tumor MR images. This phenomenon has also been shown to apply MPI, where subcutaneous tumors were selectively highlighted [48]. In another study, the tumor could be highlighted with a tumor-to-background ratio of up to 50 at the peak uptake of 6 hours after tracer injection [49].

3.1.4. Functional MPI—Functional MRI (fMRI) can be performed using either the blood-agent level-dependent (BALD) or blood-oxygenation level (BOLD) mechanism, both of which are semi-quantitative. The first method relies on injection of an MR contrast agent through which changes in blood volume can be detected upon cerebral activation. The BALD approach has been abandoned a long time ago in favor of BOLD imaging, as the latter does not require administration of a contrast agent. The same principle can be applied to MPI: by injecting SPIO as a vascular tracer, the overall MPI signal will correspond directly to the total blood volume. In theory, functional MPI (fMPI) has the advantage over fMRI in that it is truly quantitative, and whole brain cerebral blood volume (CBV) maps could possibly be automatically generated. Such initial studies on showing the feasibility of fMPI have now been reported. (Figure 6)[50].

3.1.5. Lung MPI—With ^1H MRI, the hypointensities caused by SPIO particles cannot be distinguished from the air-filled hypointense lung. This precludes ^1H MRI biodistribution studies where the lung is one of the major target organs, i.e., as is the case for the initial distribution of intravenously injected stem cells. In this scenario, MPI has a real advantage, as SPIO detection is possible in all tissues with an equal sensitivity, as exemplified for the lung in Figure 4. This enables new MPI applications for the lung, including the study of (impaired) lung perfusion [51], or inhalation of aerosolized SPIO formulations [52], which was suggested to possibly serve as an alternative mucociliary clearance test. While ^{19}F MRI avoids the problems encountered with ^1H MRI and has been successfully used for lung ventilation imaging using fluorinated gases, it suffers from low sensitivity [53]. Similar to ^{19}F MRI, MPI may also be used to visualize SPIO in areas of traumatic injury and/or hemorrhage, where endogenous deoxyhemoglobin and methemoglobin already induce tissue hypointensities on ^1H MRI. Since the iron present in these two bleeding byproducts is not superparamagnetic, it will be able to produce a specific MPI signal. Similarly, MPI can be properly used in abdominal studies [54], where the colon and other parts of the GI system often contain air-filled pockets or food packages that show up hypointense on MRI.

3.1.6. MPI-guided hyperthermia—When performing hyperthermia for treatment of cancer, the surrounding normal tissue (i.e., the liver or spleen) often suffers from collateral heat damage. More specific image-guided treatment of the actual cancer tissue is highly desirable. Using MPI to precisely determine the location of SPIO before heating may overcome these limitations through an image-guided theranostic platform (Figure 7)[55–57]. To proof this, localization of thermal damage and therapy was validated with luciferase activity and histological assessment [55]. Apart from localizing thermal therapy, this technique could possibly further extended to localize actuation of drug release and other biomechanical-based therapies.

3.2. Pros and cons of MPI compared to other *in vivo* imaging modalities

An overview of the main pros and cons of MPI compared to existing imaging modalities is given in Table 1. The primary advantages of MPI are its true quantification, promised (but yet to be proven) high sensitivity, and lack of background signal, facilitating image interpretation. In contrast to MRI, it also allows imaging applications in hemorrhagic tissue and air-tissue interfaces (i.e., skin surface, lung, and bowel studies). The main disadvantage of MPI is its lack of anatomical information, and therefore it is preferably be combined with either CT or MRI, calling for proper co-registration image post-processing procedures. Indeed, industrial efforts are underway to build an MPI/MRI scanner [58]. However, while PET/CT or SPECT/CT and PET/MRI studies are now performed routinely, PET and SPECT alone as radioactive tracer techniques are still being used today in many clinical scenarios. The spatial resolution depends on the uniformity of the size of the SPIO tracer, and hence will vary between studies using different particles. The voxel size of approximately 1 mm^3 is far less than pre-clinical ^1H MRI but approaches that of ^{19}F MRI and PET. Finally, and this should not be underestimated, the necessity of using nanosized SPIO particles will prevent many applications familiar to nuclear medicine, due to the pharmacokinetic laws related to sheer size, blood clearance, and non-specific uptake by the reticulo-endothelial system.

3.3 Future MPI opportunities and challenges

There is plenty of research space to further develop the field of MPI. Engineers are thrilled to build a clinical machine [59, 60]. Medical imaging physicists have been very active in designing improved acquisition and reconstruction techniques [61–68], much like the early days of MRI (i.e., pulse sequence development, k-space). Inorganic chemists are going back to the lab to synthesize optimized, uniformly sized superparamagnetic nanoparticles with maximum magnetic moment [69–72], similar to that pursued during the birth of SPIO MRI contrast agents in the mid 1980s. It has already been shown that, while equally effective in generating MRI contrast, certain particles can induce dramatically improved MPI signal, regardless of an intracellular or extracellular location [19]. Finally, with all optimal instrumentation, SPIO particles, and image formation in place, it will be the time for molecular and cellular biologists and pharma drug chemists to take MPI to the next level and make new biological discoveries or drug treatments. At present, we are at the very beginning of exploring MPI. If an analogy can be made to MRI and we look back, much has happened in the field of MRI during the 30 years since SPIO agents were introduced, including several successful clinical applications. This is an exciting time, and we will have to be patient to realize the full potential of MPI.

4. Clinical MPI?

A clinical MPI prototype scanner does not exist although there are no theoretical limits towards building a clinical MPI instrument [73]. Wald et al. are developing a human functional MPI scanner [59], and Magnetic Insight has also launched an initiative to build one. A main consideration for future clinical translation is the availability of a clinically approved SPIO tracer. One is Resovist, which has been widely used in MPI; it is still made and sold in Japan, and marketed by Magnetic Insight as “Vivotrax”. Feraheme (ferumoxytol) is another ultrasmall (USPIO) product that is clinically used for iron anemia/deficiency and may have potential for MPI, although likely with less sensitivity due to its smaller size. Figure 8 shows which clinical SPIO products are currently used and where. While MPI-optimized and fine-tuned SPIO particles will have to undergo a lengthy and costly path towards clinical approval, the existence of several clinical SPIO products should spur further clinical development.

Acknowledgements

For developing MPI cell tracking, the author has been supported by the National Institutes of Health (EUREKA R01 DA26299) and a grant from Philips Healthcare, Inc.

Competing interest statement

The author receives grant support from Philips Electronics North America Corp.

Abbreviation

BALD	blood agent level-dependent
BOLD	blood oxygenation level-dependent

CBV	cerebral blood volume
CEST	chemical exchange saturation transfer
CT	computed tomography
EPR	enhanced-permeability and retention
FFL	field-free line
FFP	field-free point
fMPI	functional magnetic particle imaging
FOV	field-of-view
MSC	mesenchymal stem cell
MPI	magnetic particle imaging
MPS	magnetic particle spectroscopy
MRI	magnetic resonance imaging
NSC	neural stem cell
PET	positron emission tomography
SPECT	single photon microscopy
SPIO	superparamagnetic iron oxide
TBI	traumatic brain injury

References

- [1]. Gleich B, Verfahren zur Ermittlung der räumlichen Verteilung magnetischer Partikel EP1304542A2, (2001).
- [2]. Gleich B, Weizenecker J, Tomographic imaging using the nonlinear response of magnetic particles, *Nature*, 435 (2005) 1214–1217. [PubMed: 15988521]
- [3]. Goodwill PW, Conolly SM, Multidimensional x-space magnetic particle imaging, *IEEE Trans Med Imaging*, 30 (2011) 1581–1590. [PubMed: 21402508]
- [4]. Ohgushi M, Nagayama K, Wada A, Dextran-magnetite: A new relaxation agent and its application to T2 measurements in gel systems, *J. Magn. Reson*, 29 (1978) 599–561.
- [5]. Mendonca Dias MH, Lauterbur PC, Ferromagnetic particles as contrast agents for magnetic resonance imaging of liver and spleen, *Magnetic resonance in medicine*, 3 (1986) 328–330. [PubMed: 3713497]
- [6]. Olsson MBE, Persson BRB, Salford LG, Schroder U, Ferromagnetic particles as contrast agent in T2 NMR imaging, *Magn Reson Imag*, 4 (1986) 437–440.
- [7]. Renshaw PF, Owen CS, McLaughlin AC, Frey TG, Leigh JS, Jr., Ferromagnetic contrast agents: a new approach, *Magnetic resonance in medicine*, 3 (1986) 217–225. [PubMed: 3713487]
- [8]. Bulte JW, Kraitchman DL, Iron oxide MR contrast agents for molecular and cellular imaging, *NMR Biomed*, 17 (2004) 484–499. [PubMed: 15526347]

- [9]. Fortuin AS, Bruggemann R, van der Linden J, Panfilov I, Israel B, Scheenen TWJ, Barentsz JO, Ultra-small superparamagnetic iron oxides for metastatic lymph node detection: back on the block, *Wiley Interdiscip Rev Nanomed Nanobiotechnol*, 10 (2018).
- [10]. Bulte JW, Daldrup-Link HE, Clinical tracking of cell transfer and cell transplantation: Trials and tribulations *Radiology*, (in press).
- [11]. Ahrens ET, Bulte JW, Tracking immune cells in vivo using magnetic resonance imaging, *Nat Rev Immunol*, 13 (2013) 755–763. [PubMed: 24013185]
- [12]. Bulte JW, Vymazal J, Brooks RA, Pierpaoli C, Frank JA, Frequency dependence of MR relaxation times. II. Iron oxides, *J Magn Reson Imaging*, 3 (1993) 641–648. [PubMed: 8347958]
- [13]. Bulte JW, De Jonge MW, Kamman RL, Go KG, Zuiderveen F, Blaauw B, Oosterbaan JA, The TH, de Leij L, Dextran-magnetite particles: contrast-enhanced MRI of blood-brain barrier disruption in a rat model, *Magnetic resonance in medicine*, 23 (1992) 215–223. [PubMed: 1372384]
- [14]. Bulte JW, Ma LD, Magin RL, Kamman RL, Hulstaert CE, Go KG, The TH, de Leij L, Selective MR imaging of labeled human peripheral blood mononuclear cells by liposome mediated incorporation of dextran-magnetite particles, *Magnetic resonance in medicine : official journal of the Society of Magnetic Resonance in Medicine / Society of Magnetic Resonance in Medicine*, 29 (1993) 32–37.
- [15]. Yeh TC, Zhang W, Ildstad ST, Ho C, Intracellular labeling of T-cells with superparamagnetic contrast agents, *Magnetic resonance in medicine : official journal of the Society of Magnetic Resonance in Medicine / Society of Magnetic Resonance in Medicine*, 30 (1993) 617–625.
- [16]. Bulte JW, Walczak P, Gleich B, Weizenecker J, Markov DE, Aerts HC, Boeve H, Borgert J, Kuhn M, MPI Cell Tracking: What Can We Learn from MRI?, *Proc SPIE Int Soc Opt Eng*, 7965 (2011) 79650z.
- [17]. Bulte JW, Gleich B, Weizenecker J, Bernard S, Walczak P, Markov DE, Aerts HC, Borgert J, Boeve H, Developing cellular MPI: Initial experience, *Proc. of ISMRM*, 16 (2008) 1675.
- [18]. Khandhar AP, Ferguson RM, Arami H, Krishnan KM, Monodisperse magnetite nanoparticle tracers for in vivo magnetic particle imaging, *Biomaterials*, 34 (2013) 3837–3845. [PubMed: 23434348]
- [19]. Bulte JW, Walczak P, Janowski M, Krishnan KM, Arami H, Halkola A, Gleich B, Rahmer J, Quantitative “Hot Spot” Imaging of Transplanted Stem Cells using Superparamagnetic Tracers and Magnetic Particle Imaging (MPI), *Tomography*, 1 (2015) 91–97. [PubMed: 26740972]
- [20]. Zheng B, Vazin T, Goodwill PW, Conway A, Verma A, Saritas EU, Schaffer D, Conolly SM, Magnetic Particle Imaging tracks the long-term fate of in vivo neural cell implants with high image contrast, *Scientific reports*, 5 (2015) 14055. [PubMed: 26358296]
- [21]. Zheng B, von See MP, Yu E, Gunel B, Lu K, Vazin T, Schaffer DV, Goodwill PW, Conolly SM, Quantitative Magnetic Particle Imaging Monitors the Transplantation, Biodistribution, and Clearance of Stem Cells In Vivo, *Theranostics*, 6 (2016) 291–301. [PubMed: 26909106]
- [22]. Chin BB, Nakamoto Y, Bulte JW, Pittenger MF, Wahl R, Kraitchman DL, 111In oxine labelled mesenchymal stem cell SPECT after intravenous administration in myocardial infarction, *Nucl Med Commun*, 24 (2003) 1149–1154. [PubMed: 14569169]
- [23]. Kraitchman DL, Tatsumi M, Gilson WD, Ishimori T, Kedziorek D, Walczak P, Segars WP, Chen HH, Fritzges D, Izbudak I, Young RG, Marcelino M, Pittenger MF, Solaiyappan M, Boston RC, Tsui BM, Wahl RL, Bulte JW, Dynamic imaging of allogeneic mesenchymal stem cells trafficking to myocardial infarction, *Circulation*, 112 (2005) 1451–1461. [PubMed: 16129797]
- [24]. Wang P, Goodwill PW, Pandit P, Gaudet J, Ross A, Wang J, Yu E, Hensley DW, Doyle TC, Contag CH, Conolly S, Moore A, Magnetic particle imaging of islet transplantation in the liver and under the kidney capsule in mouse models, *Quant Imaging Med Surg*, 8 (2018) 114–122. [PubMed: 29675353]
- [25]. Song G, Chen M, Zhang Y, Cui L, Qu H, Zheng X, Wintermark M, Liu Z, Rao J, Janus Iron Oxides @ Semiconducting Polymer Nanoparticle Tracer for Cell Tracking by Magnetic Particle Imaging, *Nano Lett*, 18 (2018) 182–189. [PubMed: 29232142]

- [26]. Graeser M, Knopp T, Szwargulski P, Friedrich T, von Gladiss A, Kaul M, Krishnan KM, Ittrich H, Adam G, Buzug TM, Towards Picogram Detection of Superparamagnetic Iron-Oxide Particles Using a Gradiometric Receive Coil, *Scientific reports*, 7 (2017) 6872. [PubMed: 28761103]
- [27]. Shapiro EM, Sharer K, Skrtic S, Koretsky AP, In vivo detection of single cells by MRI, *Magnetic resonance in medicine*, 55 (2006) 242–249. [PubMed: 16416426]
- [28]. Heyn C, Ronald JA, Ramadan SS, Snir JA, Barry AM, MacKenzie LT, Mikulis DJ, Palmieri D, Bronder JL, Steeg PS, Yoneda T, MacDonald IC, Chambers AF, Rutt BK, Foster PJ, In vivo MRI of cancer cell fate at the single-cell level in a mouse model of breast cancer metastasis to the brain, *Magnetic resonance in medicine*, 56 (2006) 1001–1010. [PubMed: 17029229]
- [29]. Lemaster JE, Chen F, Kim T, Hariri A, Jokerst JV, Development of a Trimodal Contrast Agent for Acoustic and Magnetic Particle Imaging of Stem Cells, *ACS Applied Nano Materials*, 1 (2018) 1321–1331.
- [30]. Haegele J, Vaalma S, Panagiotopoulos N, Barkhausen J, Vogt FM, Borgert J, Rahmer J, Multi-color magnetic particle imaging for cardiovascular interventions, *Physics in medicine and biology*, 61 (2016) N415–426. [PubMed: 27476675]
- [31]. Rahmer J, Wirtz D, Bontus C, Borgert J, Gleich B, Interactive Magnetic Catheter Steering With 3-D Real-Time Feedback Using Multi-Color Magnetic Particle Imaging, *IEEE Trans Med Imaging*, 36 (2017) 1449–1456. [PubMed: 28287965]
- [32]. Han SH, Cho E, Lee DK, Cho G, Kim YR, Cho H, Simulational validation of color magnetic particle imaging (cMPI), *Physics in medicine and biology*, 59 (2014) 6521–6536. [PubMed: 25309980]
- [33]. Rahmer J, Halkola A, Gleich B, Schmale I, Borgert J, First experimental evidence of the feasibility of multi-color magnetic particle imaging, *Physics in medicine and biology*, 60 (2015) 1775–1791. [PubMed: 25658130]
- [34]. Stehning C, Gleich B, Rahmer J, Simultaneous magnetic particle imaging (MPI) and temperature mapping using multi-color MPI, *Int. J. Magn. Part. Imaging*, 2 10.18416/ijmpi.12016.1612001.
- [35]. Ferrauto G, Delli Castelli D, Terreno E, Aime S, In vivo MRI visualization of different cell populations labeled with PARACEST agents, *Magnetic resonance in medicine*, 69 (2013) 1703–1711. [PubMed: 22837028]
- [36]. Liu G, Moake M, Har-el YE, Long CM, Chan KW, Cardona A, Jamil M, Walczak P, Gilad AA, Sgouros G, van Zijl PC, Bulte JW, McMahon MT, In vivo multicolor molecular MR imaging using diamagnetic chemical exchange saturation transfer liposomes, *Magnetic resonance in medicine*, 67 (2012) 1106–1113. [PubMed: 22392814]
- [37]. Trillaud H, Degreze P, Mesplede Y, Douws C, Palussiere J, Grenier N, Evaluation of experimentally induced renal hypoperfusion using iron oxide particles and fast magnetic resonance imaging, *Acad Radiol*, 2 (1995) 293–299. [PubMed: 9419565]
- [38]. Ludewig P, Gdaniec N, Sedlacik J, Forkert ND, Szwargulski P, Graeser M, Adam G, Kaul MG, Krishnan KM, Ferguson RM, Khandhar AP, Walczak P, Fiehler J, Thomalla G, Gerloff C, Knopp T, Magnus T, Magnetic Particle Imaging for Real-Time Perfusion Imaging in Acute Stroke, *ACS Nano*, 11 (2017) 10480–10488. [PubMed: 28976180]
- [39]. Orendorff R, Peck AJ, Zheng B, Shirazi SN, Matthew Ferguson R, Khandhar AP, Kemp SJ, Goodwill P, Krishnan KM, Brooks GA, Kaufer D, Conolly S, First in vivo traumatic brain injury imaging via magnetic particle imaging, *Physics in medicine and biology*, 62 (2017) 3501–3509. [PubMed: 28378708]
- [40]. Weizenecker J, Gleich B, Rahmer J, Dahnke H, Borgert J, Three-dimensional real-time in vivo magnetic particle imaging, *Physics in medicine and biology*, 54 (2009) L1–L10. [PubMed: 19204385]
- [41]. Kaul MG, Salamon J, Knopp T, Ittrich H, Adam G, Weller H, Jung C, Magnetic particle imaging for in vivo blood flow velocity measurements in mice, *Physics in medicine and biology*, 63 (2018) 064001. [PubMed: 29465412]
- [42]. Rahmer J, Antonelli A, Sfara C, Tiemann B, Gleich B, Magnani M, Weizenecker J, Borgert J, Nanoparticle encapsulation in red blood cells enables blood-pool magnetic particle imaging hours after injection, *Physics in medicine and biology*, 58 (2013) 3965–3977. [PubMed: 23685712]

- [43]. Antonelli A, Sfara C, Rahmer J, Gleich B, Borgert J, Magnani M, Red blood cells as carriers in magnetic particle imaging, *Biomed Tech (Berl)*, 58 (2013) 517–525. [PubMed: 23839809]
- [44]. Takeuchi Y, Suzuki H, Sasahara H, Ueda J, Yabata I, Itagaki K, Saito S, Murase K, Encapsulation of iron oxide nanoparticles into red blood cells as a potential contrast agent for magnetic particle imaging, *Adv. Biomed. Eng.*, 3 (2014) 37–43.
- [45]. Schleich N, Po C, Jacobs D, Ucar B, Gallez B, Danhier F, Preat V, Comparison of active, passive and magnetic targeting to tumors of multifunctional paclitaxel/SPIO-loaded nanoparticles for tumor imaging and therapy, *J Control Release*, 194 (2014) 82–91. [PubMed: 25178270]
- [46]. Lei XG, Jockusch S, Turro NJ, Tomalia DA, Ottaviani MF, EPR characterization of gadolinium(III)-containing-PAMAM-dendrimers in the absence and in the presence of paramagnetic probes, *J Colloid Interface Sci*, 322 (2008) 457–464. [PubMed: 18439615]
- [47]. Cheng Y, Zhao L, Li Y, Xu T, Design of biocompatible dendrimers for cancer diagnosis and therapy: current status and future perspectives, *Chem Soc Rev*, 40 (2011) 2673–2703. [PubMed: 21286593]
- [48]. Arami H, Teeman E, Troksa A, Bradshaw H, Saatchi K, Tomitaka A, Gambhir SS, Hafeli UO, Liggitt D, Krishnan KM, Tomographic magnetic particle imaging of cancer targeted nanoparticles, *Nanoscale*, 9 (2017) 18723–18730. [PubMed: 29165498]
- [49]. Yu EY, Bishop M, Zheng B, Ferguson RM, Khandhar AP, Kemp SJ, Krishnan KM, Goodwill PW, Conolly SM, Magnetic Particle Imaging: A Novel in Vivo Imaging Platform for Cancer Detection, *Nano Lett*, 17 (2017) 1648–1654. [PubMed: 28206771]
- [50]. Cooley CZ, Mandeville JB, Mason EE, Mandeville ET, Wald LL, Rodent Cerebral Blood Volume (CBV) changes during hypercapnia observed using Magnetic Particle Imaging (MPI) detection, *NeuroImage*, 178 (2018) 713–720. [PubMed: 29738908]
- [51]. Zhou XY, Jeffris KE, Yu EY, Zheng B, Goodwill PW, Nahid P, Conolly SM, First in vivo magnetic particle imaging of lung perfusion in rats, *Physics in medicine and biology*, 62 (2017) 3510–3522. [PubMed: 28218614]
- [52]. Tay ZW, Chandrasekharan P, Zhou XY, Yu E, Zheng B, Conolly S, In vivo tracking and quantification of inhaled aerosol using magnetic particle imaging towards inhaled therapeutic monitoring, *Theranostics*, 8 (2018) 3676–3687. [PubMed: 30026874]
- [53]. Ruiz-Cabello J, Barnett BP, Bottomley PA, Bulte JW, Fluorine (19F) MRS and MRI in biomedicine, *NMR Biomed*, 24 (2011) 114–129. [PubMed: 20842758]
- [54]. Yu EY, Chandrasekharan P, Berzon R, Tay ZW, Zhou XY, Khandhar AP, Ferguson RM, Kemp SJ, Zheng B, Goodwill PW, Wendland MF, Krishnan KM, Behr S, Carter J, Conolly SM, Magnetic Particle Imaging for Highly Sensitive, Quantitative, and Safe in Vivo Gut Bleed Detection in a Murine Model, *ACS Nano*, 11 (2017) 12067–12076. [PubMed: 29165995]
- [55]. Tay ZW, Chandrasekharan P, Chiu-Lam A, Hensley DW, Dhavalikar R, Zhou XY, Yu EY, Goodwill PW, Zheng B, Rinaldi C, Conolly SM, Magnetic Particle Imaging-Guided Heating in Vivo Using Gradient Fields for Arbitrary Localization of Magnetic Hyperthermia Therapy, *ACS Nano*, 12 (2018) 3699–3713. [PubMed: 29570277]
- [56]. Kuboyabu T, Yamawaki M, Aoki M, Ohki A, Murase K, Quantitative evaluation of tumor early response to magnetic hyperthermia combined with vascular disrupting therapy using magnetic particle imaging, *Int. J. Nanomed. Nanosurg.*, 2 (2016) 1–7.
- [57]. Hensley D, Tay ZW, Dhavalikar R, Zheng B, Goodwill P, Rinaldi C, Conolly S, Combining magnetic particle imaging and magnetic fluid hyperthermia in a theranostic platform, *Physics in medicine and biology*, 62 (2017) 3483–3500. [PubMed: 28032621]
- [58]. Franke J, Heinen U, Lehr H, Weber A, Jaspard F, Ruhm W, Heidenreich M, Schulz V, System Characterization of a Highly Integrated Preclinical Hybrid MPI-MRI Scanner, *IEEE Trans Med Imaging*, 35 (2016) 1993–2004. [PubMed: 26991821]
- [59]. Mason EE, Cooley CZ, Cauley SF, Griswold MA, Conolly SM, Wald LL, Design analysis of an MPI human functional brain scanner, *International journal on magnetic particle imaging*, 3 (2017).
- [60]. Top CB, Ilbey S, Guven HE, Electronically rotated and translated field-free line generation for open bore magnetic particle imaging, *Med Phys*, 44 (2017) 6225–6238. [PubMed: 28972267]

- [61]. Knopp T, Sattel TF, Biederer S, Rahmer J, Weizenecker J, Gleich B, Borgert J, Buzug TM, Model-based reconstruction for magnetic particle imaging, *IEEE Trans Med Imaging*, 29 (2010) 12–18. [PubMed: 19435678]
- [62]. Straub M, Schulz V, Joint Reconstruction of Tracer Distribution and Background in Magnetic Particle Imaging, *IEEE Trans Med Imaging*, 37 (2018) 1192–1203. [PubMed: 29727282]
- [63]. Storath M, Brandt C, Hofmann M, Knopp T, Salamon J, Weber A, Weinmann A, Edge Preserving and Noise Reducing Reconstruction for Magnetic Particle Imaging, *IEEE Trans Med Imaging*, 36 (2017) 74–85. [PubMed: 27455521]
- [64]. Gdaniec N, Szwargulski P, Knopp T, Fast multiresolution data acquisition for magnetic particle imaging using adaptive feature detection, *Med Phys*, 44 (2017) 6456–6460. [PubMed: 29044632]
- [65]. Weber A, Werner F, Weizenecker J, Buzug TM, Knopp T, Artifact free reconstruction with the system matrix approach by overscanning the field-free-point trajectory in magnetic particle imaging, *Physics in medicine and biology*, 61 (2016) 475–487. [PubMed: 26682648]
- [66]. Tateo A, Iurino A, Settanni G, Andrisani A, Stifanelli PF, Larizza P, Mazzia F, Mininni RM, Tangaro S, Bellotti R, Hybrid x-space: a new approach for MPI reconstruction, *Physics in medicine and biology*, 61 (2016) 4061–4077. [PubMed: 27164361]
- [67]. Knopp T, Hofmann M, Online reconstruction of 3D magnetic particle imaging data, *Physics in medicine and biology*, 61 (2016) N257–267. [PubMed: 27182668]
- [68]. Lu K, Goodwill P, Zheng B, Conolly S, Multi-channel Acquisition for Isotropic Resolution in Magnetic Particle Imaging, *IEEE Trans Med Imaging*, (2017).
- [69]. Khandhar AP, Ferguson RM, Arami H, Krishnan KM, Monodisperse magnetite nanoparticle tracers for in vivo magnetic particle imaging, *Biomaterials*, 34 (2013) 3837–3845. [PubMed: 23434348]
- [70]. Khandhar AP, Ferguson RM, Arami H, Kemp SJ, Krishnan KM, Tuning surface coatings of optimized magnetite nanoparticle tracers for in vivo Magnetic Particle Imaging, *IEEE Trans Magn*, 51 (2015).
- [71]. Eberbeck D, Dennis CL, Huls NF, Krycka KL, Gruttner C, Westphal F, Multicore magnetic nanoparticles for magnetic particle imaging, *IEEE Trans. Magn*, 49 (2013) 269–274.
- [72]. Ferguson RM, Khandhar AP, Kemp SJ, Arami H, Saritas EU, Croft LR, Konkle J, Goodwill PW, Halkola A, Rahmer J, Borgert J, Conolly SM, Krishnan KM, Magnetic particle imaging with tailored iron oxide nanoparticle tracers, *IEEE Trans Med Imaging*, 34 (2015) 1077–1084. [PubMed: 25438306]
- [73]. Borgert J, Schmidt JD, Schmale I, Bontus C, Gleich B, David B, Weizenecker J, Jockram J, Lauruschkat C, Mende O, Heinrich M, Halkola A, Bergmann J, Woywode O, Rahmer J, Perspectives on clinical magnetic particle imaging, *Biomed Tech (Berl)*, 58 (2013) 551–556. [PubMed: 24025718]

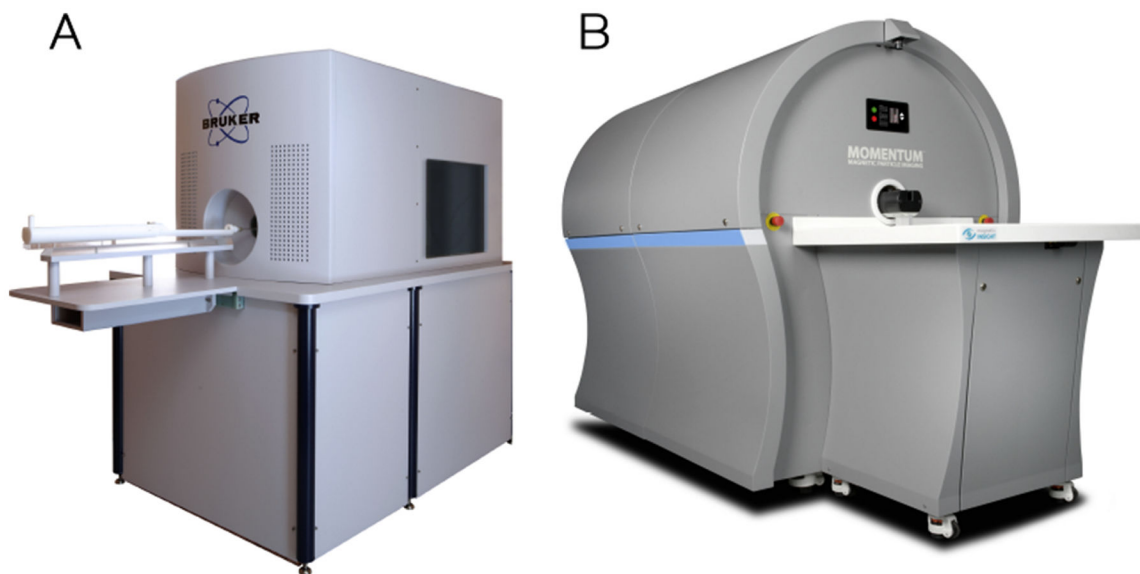


Figure 1:

The currently available two MPI systems. **(A)** Preclinical Bruker MPI system designed for 3D high temporal resolution real-time imaging applications with up to 46 volumes per second. With a bore diameter of 12 cm, the scanner is applicable for *in vivo* imaging from mice- to rabbit-size animals. The magnetic field generator is equipped with 7 individual electromagnets allowing for flexible sequence design by means of one scalable selection gradient field of up to 2.5 T/m featuring a field free point (FFP), three orthogonal drive fields for particle excitation (~25 kHz and up to ± 14 mT/ ± 14 mT/ ± 14 mT) and particle signal reception (bandwidth up to 1.25 MHz) as well as three orthogonal focus fields for slow field shifts (± 18 / ± 18 / ± 42 mT). Imaging speed is maximized by using a FFP main magnet, giving an order of magnitude higher temporal resolution than imagers using FFL magnets. Together with the embedded ParaVision acquisition and processing platform, the MPI 25/20FF offers intuitive study planning, data acquisition and reconstruction as well as automatic system control. **(B)** Magnetic Insight Momentum MPI system designed for 2D high sensitivity imaging. With a bore size of 6 cm, the scanner is applicable for *in vivo* imaging of mice. The resolution of the system is driven by a selection field gradient strength of 6.2 T/m, featuring a transmit/receive subsystem (45 kHz drive, ± 15 mT / ± 15 mT) and slow shift fields of ± 190 mT). Sensitivity is maximized by using a field free line (FFL) main magnet, giving an order of magnitude more signal than imagers using FFP magnets. System siting requires only power and cooling water, and does not require a shield room. The user experience offers one-click image acquisition and native DICOM support.

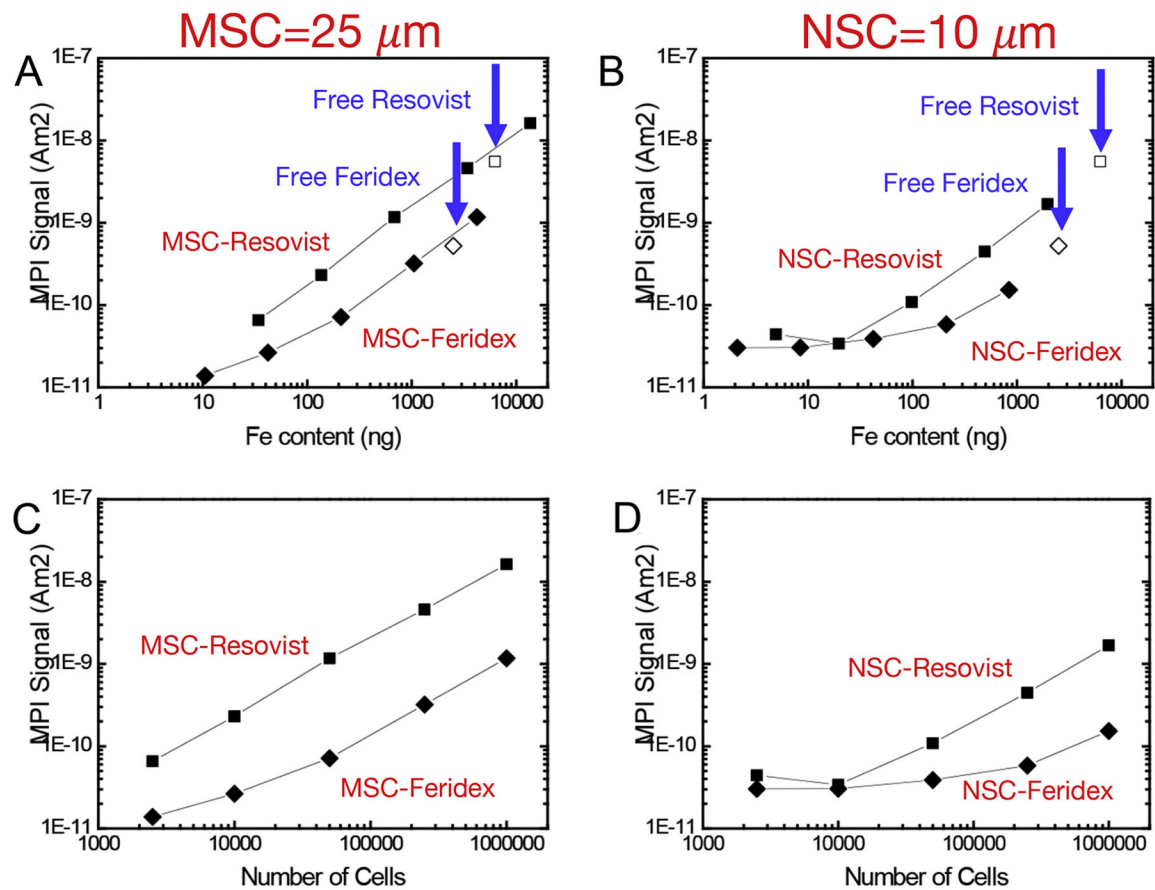


Figure 2:

First MPS measurements of stem cells labeled with commercial, clinically used SPIO formulations. Shown are the MPI signal amplitudes as a function of Fe content (**A**, **B**) and the corresponding number of cells (**C**, **D**). Data are shown for MSCs labeled with Resovist® (MR) and Feridex® (MF), and NSCs labeled with Resovist® (CR) and Feridex® (CF). Note the linearity of the MPS signal with both the iron content and number of cells except for the lowest concentration of the smaller NSCs (2,500 cells) that contain less iron. Reference samples (free, non-cell bound particles in gelatin) are included in A and B as open symbols, with no difference in signal from cell-internalized particles. Image reproduced, with permission, from Refs. [17, 19].

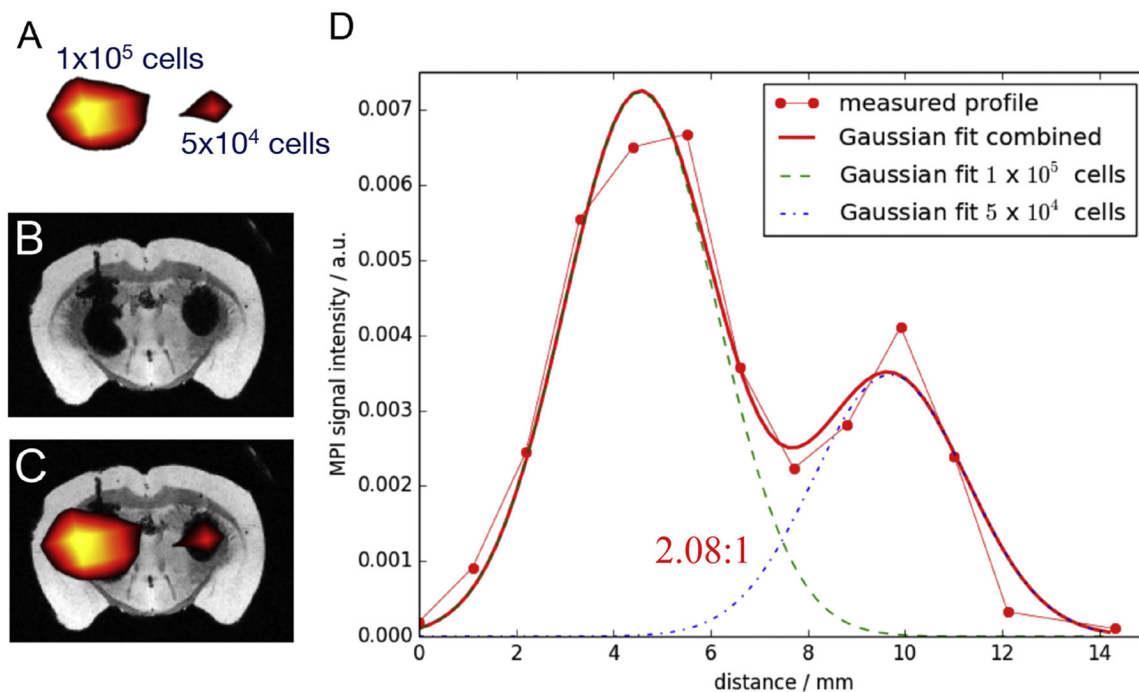


Figure 3:

First MPI/MRI cell tracking studies. MPI (A), MRI (B) and corresponding overlay MPI/MRI (C) of a mouse brain injected with 1×10^5 (left hemisphere) or 5×10^4 (right hemisphere) SPIO-labeled MSCs as a focal point transplantation in the striatum. Quantification of MPI signal measurements (D) show an excellent correlation between the measured MPI signal and number of implanted cells ($\sim 2:1$ ratio). To this end, an intensity profile through the centers of both MPI signal peaks was extracted and fitted with two Gaussian curves. Five parameters were fitted, namely the amplitudes, positions, and one width parameter, which was assumed to be the same for both curves, as it is mainly determined by the extent of the calibration sample used for system calibration. Fitted amplitude values were 7.24×10^{-3} and 3.48×10^{-3} a.u. at 4.55 and 9.69 mm for 1×10^5 and 5×10^4 cells, respectively, with a full width (resolution) of 3.68 mm. Calculated AUC MPI SI ratios were 2.08:1. Image reproduced, with permission, from Ref. [19].

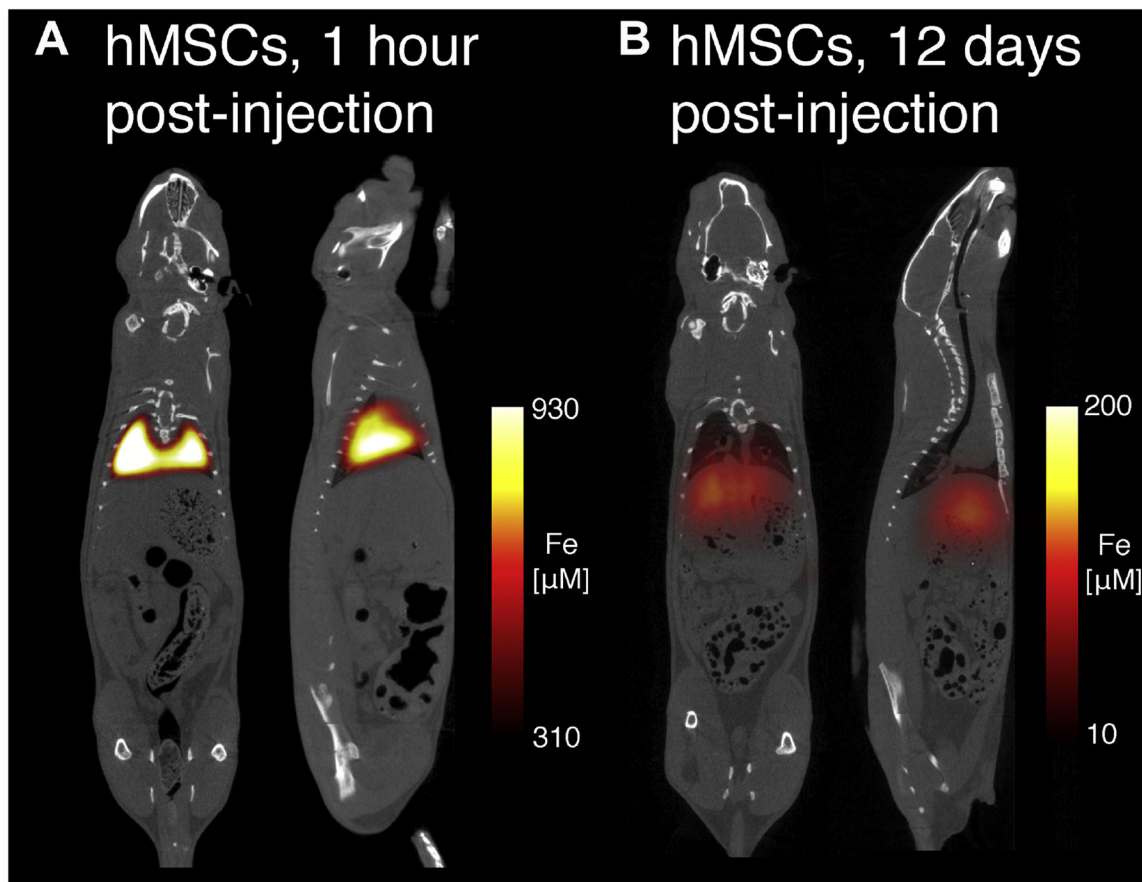


Figure 4: MPI/CT cell tracking. MPI/CT imaging of intravenously injected hMSCs, with representative coronal, sagittal, and axial slices shown from full 3D MPI datasets. **(A)** MPI imaging of hMSC tail vein injections less than 1-hour post-injection shows hMSC localization to lung only. **(B)** By 12 days, cells clear from the lung and migrate to the liver. Figure adapted from Ref. [21].

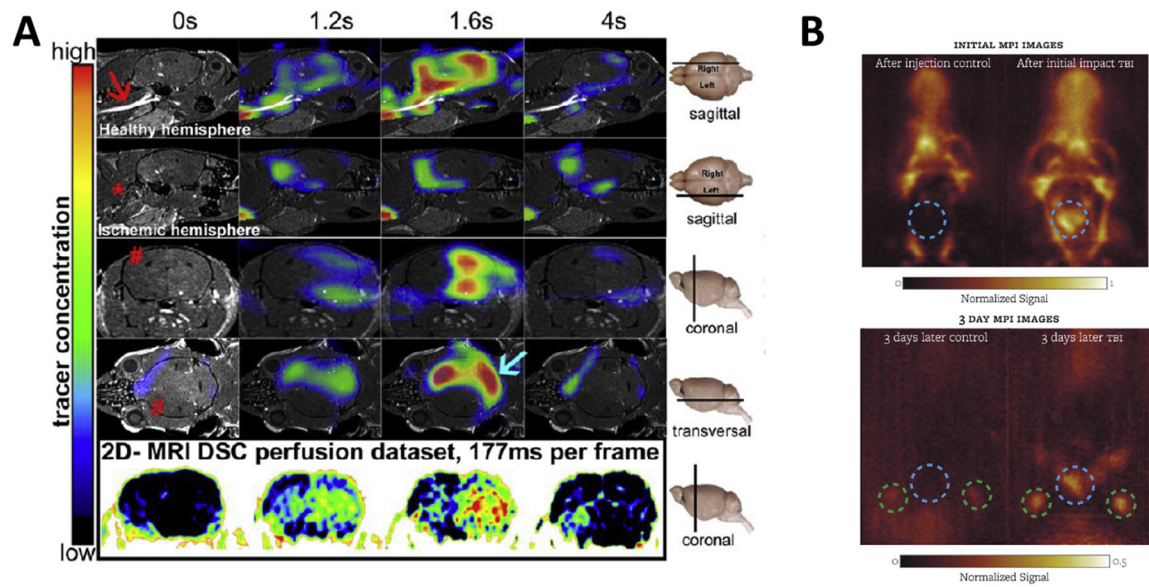


Figure 5:

MPI perfusion imaging. (A) SPIO tracer bolus passing through stroked mouse brain. Shown are slices of automatically fused 3D MPI/MRI data at several time points for the coronal, sagittal, and transverse planes. The ischemic hemisphere can be easily detected on MPI as a decreased perfusion area (red hash). Then occluded and non-occluded common/internal carotid arteries are indicated by a red asterisk and arrow, respectively. Blue arrow indicates the basil artery. MR dynamic susceptibility contrast (DSC) images are shown for comparison (bottom row). Reproduced with permission from Ref. [38]. (B) (Left). SPIO tracer bolus passing through a normal rat and a rat post traumatic brain injury (TBI). Note the large hemorrhagic brain area in the TBI animal, a result of vascular leakage. (Right) MP images obtained after three days post-injection. Blue and green circles indicate the area of the impact site and lymph nodes, respectively. Unlike the control, the TBI rat continues to have significant signal from the hemorrhage and with SPIO accumulation inside the lymph nodes. Reproduced with permission from Ref. [39].

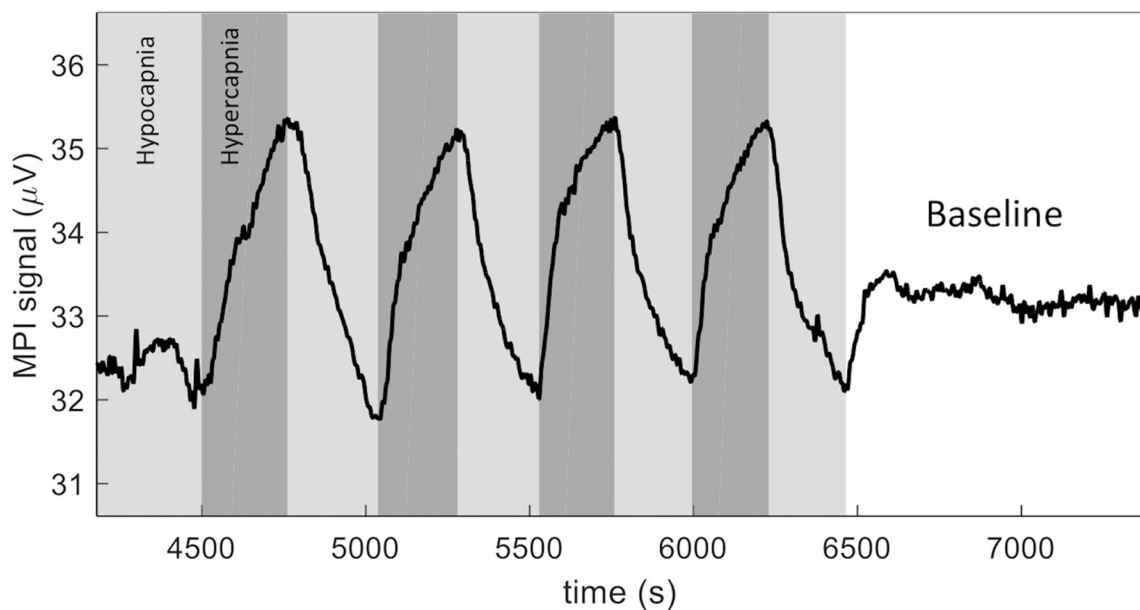


Figure 6:

Brain fMPI. MPI measurement of CBV modulated by a hypercapnic (5% CO₂) paradigm in a rat model. Ventilation properties controlled for alternating hypo/hypercapnia in 5 min periods. The MPI signal shows a 10% signal modulation with the expected CBV trend and CNR = 50. Representative blood-gas measurements were recorded for each condition, with respiratory rate/pCO₂/pO₂ values of 55 BPM/28 mm Hg/57 mm Hg, 32 BPM/49mm Hg/47 mm Hg, and 34 BPM/35 mmHg/79mm Hg for hypocapnia, hypercapnia, and baseline, respectively. Image adapted, with permission, from Ref. [50].

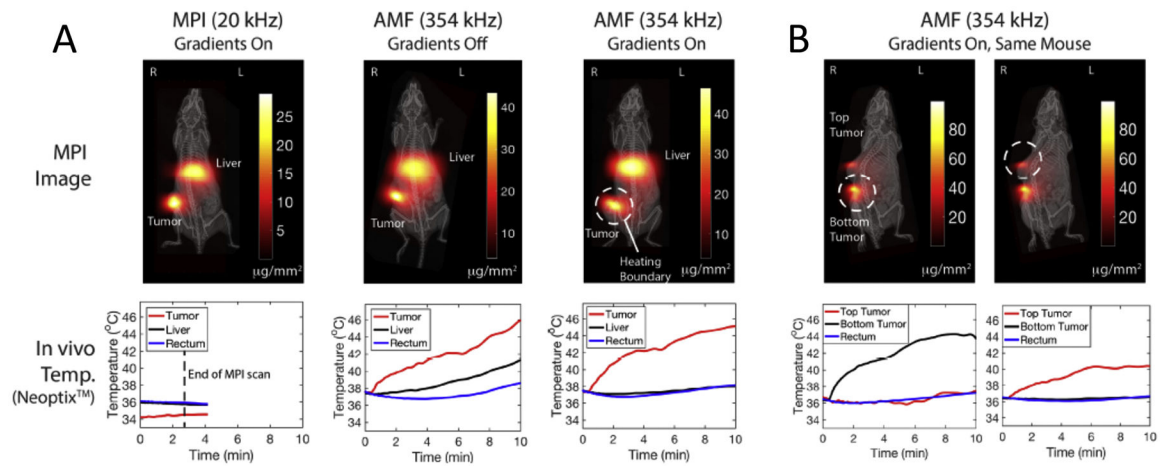


Figure 7:

MPI-guided tumor hyperthermia with sparing of normal liver tissue. During the standard MPI scan, negligible heating was observed in the mouse to the low frequency of 20 kHz. At a higher frequency of 354 kHz, all SPIO-containing tissues are heated up, including the healthy liver. When using MPI gradients, only the tumor is heated while the liver is spared. A dual tumor mouse model was then used to demonstrate arbitrary control of tumor heating. The FLL was first centered on the bottom tumor, heating the bottom tumor but not the top tumor. Without moving the animal, the FFL was then centered on the top tumor and the process was reversed. Image reproduced, with permission, from Ref. [55].

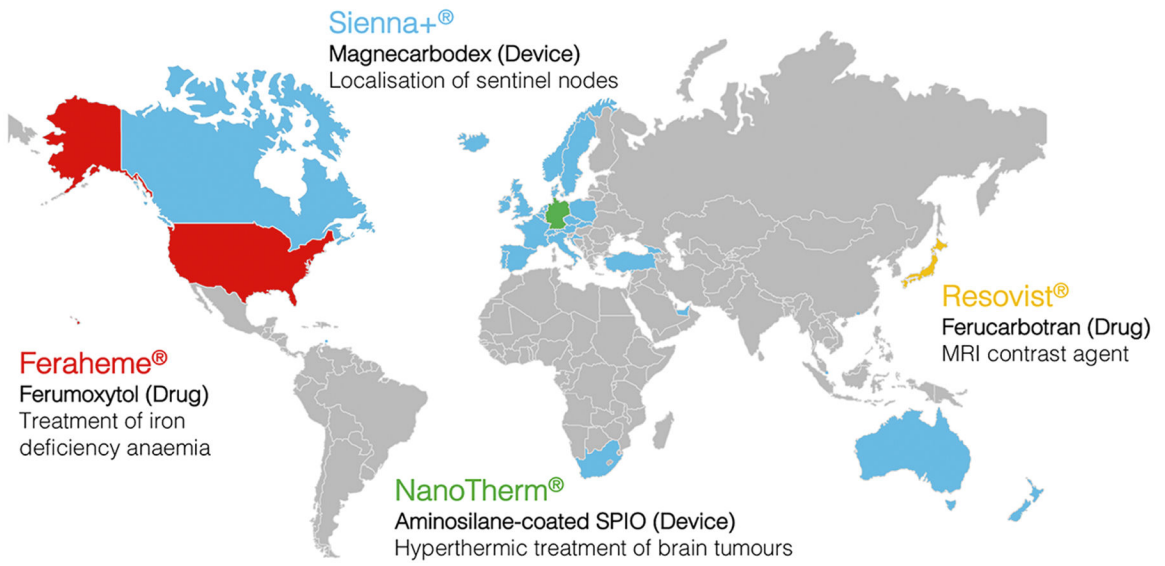


Figure 8: Geographical overview of currently clinically used commercial SPIO formulations. Image courtesy of Dr. Eric Mayes (Endomagnetics, Ltd).

Comparison of MPI to other imaging modalities that use labels (-, +, ++, and +++ represent none, weak, moderate, and strong capabilities, respectively).

Table 1:

Modality	Labeling	Type of Labeling	Detection Sensitivity	Quantitation	Resolution	Whole body imaging	Clinical use	Cost instrument ^{***}
¹ H MRI	Gd direct labeling	Contrast [*]	+		+++	+++	+/-	>1M
¹ H MRI	SPIO direct labeling	Contrast [*]	+++		+++	+++	+++	>1M
¹⁹ F MRI	¹⁹ F direct labeling	Hot spot ^{**}	+	+	+	+++	+++	>1M
PET	Direct labeling	Hot spot	+++	+	+	+++	+++	>1M [#]
PET	Reporte r gene	Hot spot	+++	+	+	+++	++	>1M [#]
SPECT	Direct labeling	Hot spot	+++	+	++	+++	+++	0.5-1M
SPECT	Reporte r gene	Hot spot	++	+	++	+++	+	0.5-1M
CT	Direct labeling	Contrast	+	+	+++	+++	-	0.1-1M
US	Direct labeling	Contrast	+	-	+	-	+	<0.1M
Optical	Direct labeling	Hot spot	+++	+/- &	+	+	+	0.1-1M
Optical	Reporte r gene	Hot spot	+++	+/- &	+	+	+/-	0.1-1M
MPI	Direct labeling	Hot spot	+++	+	-	+++	% [‡]	0.5-2M

* Marker is not detected directly, but affects indirectly the physical medium of detection (e.g. protons, acoustic reflectivity, X-ray attenuation). It therefore increases contrast, be it positive or negative.

** Marker is detected directly as a tracer (light or radioactivity as medium of detection), i.e., as a “hot spot” without background signal. Therefore, there is no anatomical information; modality often combined with other technique (i.e. MR/PET, PET/CT, SPECT/CT, or MPI/MPI and MPI/CT)

*** Pre-clinical.

[#] Costs also need to include cyclotron and salary of radiochemists.

& Tissue depth-dependent.

% No physical constraints, efforts to build a clinical machine are underway.